Naval Research Laboratory
Washington, DC 20375-5320

NRL/MR/6790--05-8907

Optimum Wavelength and Power for Efficient Laser Propagation in Various Atmospheric Environments

PHILLIP SPRANGLE
JOSEPH PEÑANO

Beam Physics Branch
Plasma Physics Division

BAHMAN HAFIZI

Icarus Research Inc.
Bethesda, Maryland

October 25, 2005

REPORT DOCUMENTATION PAGE

Form Approved
OMB No. 0704-0188

1. REPORT DATE *(DD-MM-YYYY)*	2. REPORT TYPE	3. DATES COVERED *(From - To)*
25-10-2005	Interim	10/01/2004 - Present

4. TITLE AND SUBTITLE

Optimum Wavelength and Power for Efficient Laser Propagation in Various Atmospheric Environments

5a. CONTRACT NUMBER

5b. GRANT NUMBER

5c. PROGRAM ELEMENT NUMBER

6. AUTHOR(S)

Phillip Sprangle, Joseph Peñano, and Bahman Hafizi*

5d. PROJECT NUMBER
67-8733-A5

5e. TASK NUMBER

5f. WORK UNIT NUMBER

7. PERFORMING ORGANIZATION NAME(S) AND ADDRESS(ES)

Naval Research Laboratory
4555 Overlook Avenue, SW
Washington, DC 20375-5320

8. PERFORMING ORGANIZATION REPORT NUMBER

NRL/MR/6790--05-8907

9. SPONSORING / MONITORING AGENCY NAME(S) AND ADDRESS(ES)

Joint Technology Office
901 University Blvd., SE, Suite 100
Albuquerque, NM 87106

Office of Naval Research
875 Randolph St.
Arlington, VA 22203

10. SPONSOR / MONITOR'S ACRONYM(S)

JTO & ONR

11. SPONSOR / MONITOR'S REPORT NUMBER(S)

12. DISTRIBUTION / AVAILABILITY STATEMENT

Approved for public release; distribution is unlimited.

13. SUPPLEMENTARY NOTES

*Icarus Research, Inc., 7113 Exfair Rd., Bethesda, MD 20814

14. ABSTRACT

This paper discusses the optimum laser wavelength and power for efficient propagation in maritime, desert, rural, and urban atmospheric environments. The theoretical/numerical model used in this study includes the effects of aerosol and molecular scattering, aerosol heating and vaporization, thermal blooming due to aerosol and molecular absorption, atmospheric turbulence and beam quality. These processes are modeled in a fully three-dimensional and time-dependent manner. It is found that aerosols, which consist of water, sea salt, organic matter, dust, soot, etc., are particularly important because they result in laser scattering and enhanced thermal blooming. In the water vapor transmission windows, the total absorption coefficient driving thermal blooming can be caused mainly by aerosols and not water vapor. In certain maritime environments the deleterious effects of aerosols can be reduced by vaporization. Aerosols which cannot be vaporized, e.g., dust and soot, can significantly increase thermal blooming. The laser power, averaged over dwell time, delivered to a distant target as a function of transmitted power is obtained for a number of wavelengths and atmospheric environments. The optimum wavelength and power are found for each atmospheric environment.

15. SUBJECT TERMS

Propagation; High energy lasers; Laser beam; Aerosols; Thermal blooming

16. SECURITY CLASSIFICATION OF:			17. LIMITATION OF ABSTRACT	18. NUMBER OF PAGES	19a. NAME OF RESPONSIBLE PERSON
a. REPORT	b. ABSTRACT	c. THIS PAGE			Phillip Sprangle
Unclassified	Unclassified	Unclassified	UL	44	19b. TELEPHONE NUMBER *(include area code)* (202) 767-3493

CONTENTS

Optimum Wavelength and Power for Efficient Laser Propagation in Various Atmospheric Environments

Phillip Sprangle, Joseph Peñano and Bahman Hafizi*

Plasma Physics Division

Naval Research Laboratory

Abstract

This paper addresses the key physical processes that affect the propagation of high energy lasers in the atmosphere. The main objective is to discuss the optimum laser wavelength and power for efficient propagation in maritime, desert, rural and urban atmospheric environments. The theoretical/numerical model used in this study includes the effects of aerosol and molecular scattering, aerosol heating and vaporization, thermal blooming due to aerosol and molecular absorption, atmospheric turbulence, and beam quality. These processes are modeled in a fully three-dimensional and time-dependent manner. It is found that aerosols, which consist of water, sea salt, organic matter, dust, soot, biomass smoke, urban pollutants, etc., are particularly important because they result in laser scattering, absorption and enhanced thermal blooming. In the water vapor transmission windows, the total absorption coefficient driving thermal blooming can be caused mainly by aerosols and not water vapor. In certain maritime environments the deleterious effects of aerosols can be reduced by vaporization. Aerosols which cannot be vaporized, such as those consisting of dust, soot, etc., can significantly increase thermal blooming. We show that moderate values of the laser beam quality parameter have little effect on the propagation efficiency. The laser power, averaged over dwell time, delivered to a distant target as a function of transmitted power is obtained for a number of wavelengths and atmospheric environments. The optimum wavelength and power are found for each atmospheric environment.

* Icarus Research, Inc., P.O. Box 30780, Bethesda, MD 20824-0780

Manuscript approved October 20, 2005

I. Introduction

High energy lasers (HELs) have a number of directed energy (DE) applications requiring high-intensity beams to be propagated long distances under a wide range of atmospheric conditions. The optimum wavelength for efficient HEL propagation depends on the atmospheric conditions and a number of inter-related physical processes which include: thermal blooming due to aerosol and molecular absorption [1], turbulence [2], aerosol and molecular scattering [3], thermal scattering due to heated aerosols, and aerosol heating and vaporization [4-7]. The relative importance of these processes depends on the parameters of the atmospheric environment which can vary significantly depending on location and time.

Atmospheric environments contain various types and concentrations of aerosols which can, for HEL beams, enhance thermal blooming and significantly affect the propagation efficiency. In general, aerosols consist of hygroscopic and non-hygroscopic particles of various sizes and chemical compositions. Hygroscopic aerosols are water-soluble and vary in size depending on the relative humidity [8]. Oceanic aerosols consist of sea salt, water, and organic material. Non-hygroscopic aerosols are composed of dust, soot, biomass smoke, and other carbon-based compounds. These aerosols typically have much larger absorption coefficients than water-based aerosols. While they are normally present in continental, rural and urban environments, dust aerosols can also be present in maritime environments hundreds of miles from shore [9].

Aerosols can absorb laser energy and, in the case of hygroscopic aerosols, the absorbed energy goes into both heating and vaporizing the aerosol. Heated aerosols conductively heat the surrounding air, resulting in an increase in thermal blooming of the HEL beam [10]. However, since aerosol scattering and absorption coefficients are strongly dependent on the aerosol radius, vaporizing the aerosol can improve the propagation efficiency. Non-hygroscopic aerosols (dust, soot, etc.), however, have large scattering and absorption coefficients and will not vaporize at the intensity levels anticipated in DE applications. These aerosols continually heat the surrounding air leading to significant thermal blooming.

Water vapor absorption bands and those of carbon dioxide determine the atmospheric transmission windows in the infrared. Under a range of atmospheric

conditions and laser wavelengths, aerosol absorption can exceed water vapor absorption and thus can be the dominant process for thermal blooming. For example, in a maritime environment at an operating wavelength of $\lambda = 1.045\,\mu m$, the water vapor absorption coefficient is $\sim 3\times10^{-5}\ km^{-1}$ [11] while the aerosol absorption coefficient is often greater than $10^{-3}\ km^{-1}$. In other water vapor transmission windows, i.e., 1.625 μm and 2.141 μm, the water vapor and aerosol absorption coefficients can be comparable. In addition to enhancing thermal blooming, aerosols can also significantly contribute to the total laser scattering coefficient.

In this study, the Advanced Navy Aerosol Model (ANAM) is used to model the near-surface maritime environment [12]. The ANAM aerosol distribution is comprised of various modes which represent aerosols of different compositions and sizes. Using Mie cross-sections, we calculate the absorption and scattering coefficients associated with each individual mode. The gross scattering and absorption coefficients that we obtain are comparable with *in situ* measurements [13,14] and are used for simulating aerosol induced thermal blooming and laser scattering.

In this paper the relevant processes which limit HEL propagation efficiency in maritime, desert, rural, and urban environments are analyzed. To simulate the many inter-related processes affecting atmospheric HEL propagation, we use the **h**igh **e**nergy **l**aser **c**ode for **a**tmospheric **p**ropagation HELCAP [15], developed at the Naval Research Laboratory. HELCAP models, among others, the effects of i) aerosol and molecular scattering, ii) aerosol heating and vaporization, iii) thermal blooming due to both aerosol and molecular absorption, iv) atmospheric turbulence, and v) laser beam quality. It is the first HEL propagation model which integrates all these physical processes in a fully three-dimensional, time-dependent manner. In modeling the aerosol effects, we account for the aerosol distribution and the various aerosol modes (water-based, dust, soot, etc.). Furthermore, since the thermal blooming process is modeled in a fully time-dependent manner, we can simulate propagation through stagnation zones, i.e., locations at which the wind/slew velocity is zero [16].

In Section II we estimate the relative contributions to laser beam spreading and intensity loss in a maritime environment for three wavelengths lying within the water vapor transmission window. The effects considered include: laser beam quality effects,

turbulence, molecular and aerosol thermal blooming, and aerosol thermal scattering, molecular and aerosol scattering and absorption. In Section III, the various aerosol models, e.g., NAM [17,18], ANAM [12], NAAPS [9], and our method for obtaining aerosol scattering and absorption coefficients are discussed. In Section IV, aerosol heating and vaporization and their effect on propagation are analyzed. Thermal blooming in the presence of aerosols is analyzed in Section V. In Section VI, the laser power delivered to a distant target as a function of transmitted laser power is found for a number of wavelengths and atmospheric environments. We show, among other things, that i) water vapor transmission windows are not necessarily the determining factor for choosing the optimum HEL wavelength ii) thermal blooming due to aerosol absorption can be the main contributor to beam spreading within the water vapor transmission windows iii) non-hygroscopic aerosols, because of their large absorption coefficient, and the fact that they can not be vaporized, are the main sources of aerosol absorption and hence thermal blooming and iv) moderate values of beam quality ($M^2 < 4$) have a minor effect on the propagation efficiency compared to the effects of turbulence, thermal blooming, and aerosol scattering.

II. Physical Processes Affecting HEL Propagation

The purpose of this section is to obtain estimates for the relative importance of the various physical processes that lead to transverse spreading and loss of intensity of an HEL beam. Three different laser wavelengths, $\lambda = 1.045, 1.625$ and $2.141\mu m$, all of which lie within water vapor transmission windows, are used for illustration. Full scale simulations of these interrelated processes will be presented and discussed in Sec. VI for a number of atmospheric environments. In this section we estimate these effects individually in order to better understand the results of the full scale simulations.

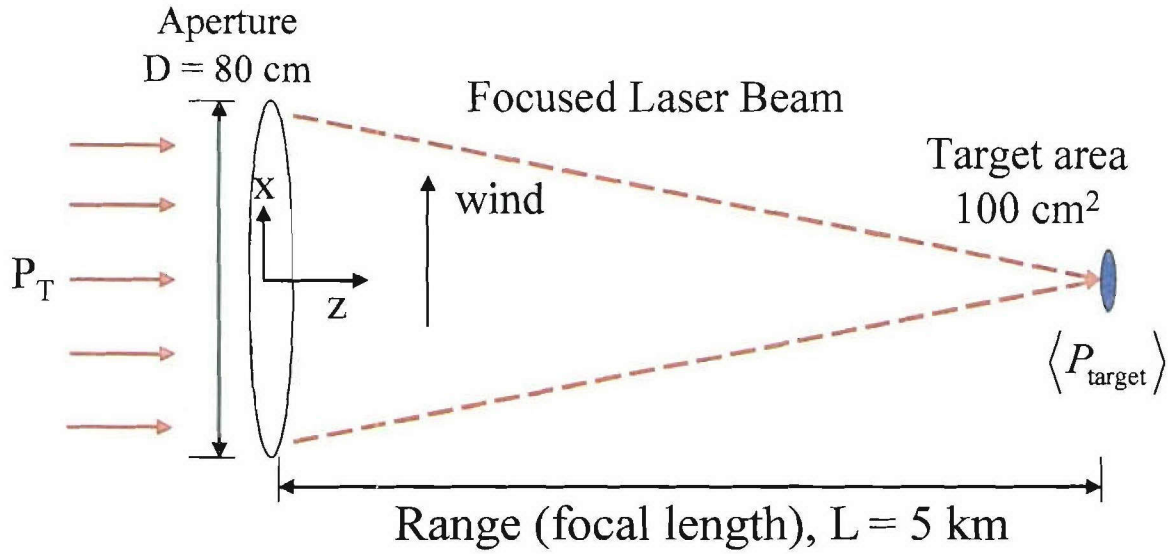

Figure 1: Schematic of laser and target configuration used in illustration and full scale simulations

Laser Wavelengths, $\lambda\ [\mu m]$	1.045, 1.625, 2.141
Laser Power, P_T[MW]	1
Laser Spot size, R_0 [cm]	50
Aperture Diameter, D[cm]	80
Peak Laser Intensity at Source, I[kW/cm^2]	0.27
Average Intensity along Path, $\langle I \rangle$ [kW/cm^2]	2
Pointing Jitter, $\Delta\Theta_{jitter}$ [μ rad]	2
Laser Beam Quality, M^2	4
Range, L[km]	5
Wind Velocity, V_w [m/sec]	5
Turbulence Strength, $C_n^2\ [m^{-2/3}]$	10^{-15}
Water Vapor Absorption Coefficient, α_{WV} [km^{-1}]	3×10^{-5}, 2×10^{-3}, 3×10^{-3}
Aerosol Scattering Coefficient, β_A [km^{-1}]	$1.2\times10^{-1}, 7\times10^{-2}, 5\times10^{-2}$
Aerosol Absorption Coefficient, α_A [km^{-1}]	2×10^{-3}, 2×10^{-3}, 3×10^{-3}
Effective Aerosol Absorption Coefficient, [km^{-1}]	1×10^{-3}

Table 1: Laser and atmospheric parameters used in illustration to estimate and compare various effects

The configuration used in the HEL propagation examples is shown in Fig. 1. An HEL beam, with an aperture diameter of 80 cm, is focused onto a target a distance of $L \sim 5$ km from the source. For illustrative purposes, we chose atmospheric parameters typical of a maritime environment. The formulas used in the illustration, however, can be applied to other atmospheric conditions. The HEL and atmospheric parameters are listed in Table 1, for three laser wavelengths.

The average laser power on the target is determined by the change in the laser spot size on target and intensity loss due to the various processes. Some processes, e.g. turbulence, are due to small angle scattering events and for our purposes are best described by a laser beam spreading angle. The HEL spreading angle is the ratio of the change in spot size to the propagation distance, i.e., $\Delta\Theta \sim \Delta R / L$. Other processes, such as molecular scattering, result in large angle scattering events and are best described by an extinction coefficient.

i) Beam Quality

It is common practice to characterize the higher order modal content of a laser beam by a beam quality parameter denoted by M^2. The quantity $M^2 \geq 1$ is a "times diffraction-limited" parameter which, for a fundamental Gaussian beam, is unity. This is one of many measures of beam quality and has a limited value in determining the far field profile. The laser spot size on the target due to finite beam quality, i.e., $M^2 = 4$, diffractive spreading is

$$\Delta R_{quality} \approx \frac{M^2 \lambda}{\pi R_0} L \approx \begin{cases} 1.1\,\text{cm}, & \text{for } 1.045\,\mu\text{m} \\ 1.7\,\text{cm}, & \text{for } 1.625\,\mu\text{m} \\ 2.2\,\text{cm}, & \text{for } 2.141\,\mu\text{m} \end{cases}. \qquad (1)$$

ii) Turbulence

Temperature and density fluctuations inherent in the atmosphere lead to random fluctuations in the refractive index. The resulting turbulence causes the laser beam to transversely spread and wander. The size distribution of the turbulence is often modeled

by a Kolmogorov distribution with structure function parameter C_n^2, which characterizes the strength of the turbulence [2]. The increase of the laser beam spot size on the target due to turbulence is given by

$$\Delta R_{turb} \approx 2\left(\frac{C_n^2 L}{\lambda^{1/3}}\right)^{3/5} L \approx \begin{cases} 2.6\,\text{cm}, & \text{for } 1.045\,\mu\text{m} \\ 2.4\,\text{cm}, & \text{for } 1.625\,\mu\text{m}. \\ 2.3\,\text{cm}, & \text{for } 2.141\,\mu\text{m} \end{cases} \quad (2)$$

Note that the radial spread, ΔR_{turb}, is weakly dependent on the wavelength, i.e., is proportional to $\lambda^{-1/5}$.

iii) Molecular scattering

The ratio of the laser intensity on a target at range L to that at the source, due to molecular scattering, is

$$I_{\text{target}} / I_{\text{source}} = \exp(-\beta_m L). \quad (3)$$

The molecular scattering coefficient β_m can be written as

$$\beta_m = n_m \sigma_m \approx \begin{cases} 7.5\times10^{-4}\,\text{km}^{-1}, & \text{for } 1.045\,\mu\text{m} \\ 1.3\times10^{-4}\,\text{km}^{-1}, & \text{for } 1.625\,\mu\text{m}, \\ 4.3\times10^{-5}\,\text{km}^{-1}, & \text{for } 2.141\,\mu\text{m} \end{cases} \quad (4)$$

where n_m is the molecular density and

$\sigma_m = (8\pi/3)\left(\pi(n_0^2-1)/n_m\lambda^2\right)^2 \approx 3.3\times10^{-28}/\lambda^4(\mu m)$ is the Rayleigh scattering cross-section. The laser intensity loss due to molecular scattering is negligible, i.e., $I_{\text{target}} / I_{\text{source}} = \exp(-\beta_m L) \approx 1$, for all three wavelengths.

iv) Aerosol scattering

The aerosol scattering coefficient is $\beta_A = \int dR\, F(R)\sigma_{scat}(R)$, where $F(R)$ is the aerosol radius distribution function and $\sigma_{scat}(R)$ is the scattering cross-section of an aerosol with radius R. The ratio of the laser intensity on a target at range L to that at the source is

$$I_{\text{target}} / I_{\text{source}} = \exp(-\beta_A L) \approx \begin{cases} 0.5, & \text{for } 1.045\,\mu\text{m} \\ 0.7, & \text{for } 1.1625\,\mu\text{m} \\ 0.8, & \text{for } 2.141\,\mu\text{m} \end{cases}. \qquad (5)$$

Aerosol scattering leads to significant loss of intensity, particularly at the shortest wavelength.

v) Aerosol thermal scattering

Aerosols absorb laser energy and heat the surrounding air through thermal conduction. The increase in air temperature has a spatially fluctuating component which can scatter the HEL beam. The uniformly heated component of the air temperature results in thermal blooming and is discussed in subsection vii). In the geometric optics limit, multiple, small-angle scatterings result in the spreading of the laser beam. The increase in the laser spot size on the target due to aerosol thermal scattering is given by

$$\Delta R_{A,T} \approx \Theta_{A,T} L$$

$$\approx 6.3\times10^{-4}\left(\frac{\alpha_D \langle I \rangle}{\kappa T_{amb}(1+\eta)}\right) n_A^{1/2} R_A^3 L^{3/2} \approx \begin{cases} 0.16\,\text{cm}, & \text{for } 1.045\ \mu\text{m} \\ 0.57\,\text{cm}, & \text{for } 1.625\,\mu\text{m} \\ 1.1\,\text{cm}, & \text{for } 2.141\,\mu\text{m} \end{cases}, \qquad (6)$$

where $\Theta_{A,T}$ is the spreading angle associated with thermal scattering, $\langle I \rangle$ is the average laser intensity along the propagation path, T_{amb} is the ambient air temperature, n_A is the number density of aerosols, R_A is the aerosol radius, α_D is the bulk absorption coefficient of the aerosols and η is a constant of order unity representing the ratio of laser energy going into vaporization to laser energy conducted into the air. In obtaining the results in Eq. (6) the following values were used, α_D = 8.4, 30 and 59 cm^{-1} for 1.045 μm, 1.625 μm and 2.141 μm, respectively.

vi) Thermal blooming due to water vapor absorption

Molecular absorption, particularly water vapor absorption, heats the air in the path of the HEL beam and results in thermal blooming. The molecular absorption coefficient is minimized by operating within the water vapor transmission window. The estimates in

this and the following subsection apply to whole beam thermal blooming in the steady state isobaric regime. An estimate for the increase in spot size on the target is

$$\Delta R_{TB,WV} \approx \alpha_{WV}\,\beta_{TB}\,\langle I\rangle\frac{L^2}{V_W} \approx \begin{cases} 0.23\,\text{cm}, & \text{for } 1.045\,\mu\text{m} \\ 15.0\,\text{cm}, & \text{for } 1.625\,\mu\text{m}, \\ 22.5\,\text{cm}, & \text{for } 2.141\,\mu\text{m} \end{cases} \tag{7}$$

α_{WV} is the water vapor absorption coefficient,

$\beta_{TB} = (n_0 - 1)/\rho_0 c_p T_0 = 7.5\times10^{-4}$ cm^3/J at STP, V_W is the wind/slew velocity, and c_p, ρ_0 and T_0 are the specific heat at constant pressure, mass density and temperature of air, respectively. It should be noted that in the presence of wind or slew the transverse intensity profile of the laser beam becomes highly asymmetric, i.e., crescent-shaped, and the above estimate for the spot size is merely an indication of the transverse scale associated with the intensity profile.

vii) Aerosol-induced thermal blooming

In addition to the thermal scattering effect discussed above, a collection of heated aerosols can also lead to enhanced thermal blooming [10]. Aerosol-induced thermal blooming is due to thermal conduction from the heated aerosols into the surrounding air. The effective absorption coefficient for aerosol-induced thermal blooming is given by $\alpha_A/(1+\eta)$ where α_A is the aerosol absorption coefficient. The increase in the laser beam spot size on the target due to aerosol-induced thermal blooming is

$$\Delta R_{TB,A} \approx \frac{\alpha_A}{1+\eta}\beta_{TB}\,\langle I\rangle\frac{L^2}{V_W} \approx \begin{cases} 4.7\,\text{cm}, & \text{for } 1.045\,\mu\text{m} \\ 4.7\,\text{cm}, & \text{for } 1.625\,\mu\text{m}. \\ 7\,\text{cm}, & \text{for } 2.141\,\mu\text{m} \end{cases} \tag{8}$$

Aerosol induced thermal blooming will be discussed in detail in Sec. V.

The contributions to the laser spot size and loss in laser intensity on target due to the various processes described above are summarized in Table 2. The laser and atmospheric parameters used in these examples are listed in Table 1 for three wavelengths which lie within the water vapor transmission windows. The contribution to the spot size increase due to beam jitter, $\Delta R_{jitter} \sim \Delta\Theta_{jitter}\,L \sim 1\,\text{cm}$, is the same for the

Wavelength, λ [μm]	1.045	1.625	2.141
Beam Quality, $\Delta R_{quality}$ [cm]	1.1	1.7	2.2
Beam Jitter, ΔR_{jitter} [cm]	1	1	1
Turbulence, ΔR_{turb} [cm]	2.6	2.4	2.3
Water Vapor, Thermal Blooming, $\Delta R_{TB,WV}$ [cm]	0.23	15	22.5
Aerosol Thermal Scattering, $\Delta R_{A,T}$ [cm]	0.16	0.57	1.1
Aerosol Induced Thermal Blooming, $\Delta R_{TB,A}$ [cm]	4.7	4.7	7
Intensity Ratio (Molecular Scattering), I_{target} / I_{source}	1	1	1
Intensity Ratio (Aerosol Scattering), I_{target} / I_{source}	0.5	0.7	0.8

Table 2. Estimates of HEL spreading and intensity loss due to various processes for three laser wavelengths

three wavelengths. Molecular (Rayleigh) scattering is practically negligible in the three cases.

Based on the above illustration we find that: i) for a laser wavelength of 1.045 μm the spread in the beam spot size is dominated by aerosol induced thermal blooming, while the intensity on target is reduced by almost 50% as a result of aerosol scattering, ii) for a laser wavelength of 1.625 μm thermal blooming due to water vapor absorption is the dominant contributor to the spread in the beam spot size, while the intensity on target is reduced by nearly 30% as a result of aerosol scattering, iii) for the case of 2.141 μm thermal blooming due to water vapor absorption is by far the largest contributor to the spread in the beam spot size, while the intensity on target is reduced by nearly 20% as a result of aerosol scattering and finally, iv) moderate values of the laser beam quality factor M^2, i.e., values less than 4, have little effect on the propagation of HELs compared to molecular/aerosol thermal blooming effects or turbulence.

Comparing the three wavelengths considered in Tables 1 and 2, aerosol scattering is more important for the shortest wavelength, 1.045 μm, while water vapor induced thermal blooming is an issue for the longest wavelength, 2.141 μm. As far as the loss in intensity due to scattering is concerned, 2.141 μm results in the largest propagation efficiency. It should be noted, however, that the results given in Table 2 are meant to be illustrative, and not necessarily typical of a maritime atmosphere.

III. Atmospheric Aerosols

As shown in the previous Section, aerosol scattering and absorption can play an important role in limiting the laser energy delivered to a remote target. In typical maritime and continental environments, the aerosol scattering and absorption coefficients can be as large as 0.2 km^{-1} and $0.01 km^{-1}$, respectively, even though the average water content of aerosols is typically far less than that of humid air. For example, at a temperature of 30 °C and relative humidity of 50%, the water vapor mass density is $\rho_{WV} \sim 1.5\times10^{-5}$ g/cm^3 while the average mass density of maritime aerosols is typically far less, $\leq 10^{-9}$ g/cm^3. However, water molecules scatter more efficiently in the form of aerosols due to the collective nature of the scattering.

Aerosols occur over a range of sizes and compositions. Maritime aerosols consist of seawater droplets with radii in the range 0.01μm – 10μm [17]. Continental aerosols are typically comprised of soot and non-hygroscopic dust, biomass smoke, and a variety of water-soluble materials [9]. There are numerous models that attempt to describe the size distribution and composition of aerosols. The Navy Aerosol Analysis and Prediction System (NAAPS) is a near-operational predictive aerosol model that uses meteorological data from the Navy Operational Global Atmospheric Prediction System (NOGAPS) to forecast aerosol concentrations in real time. It has extensive microphysics and chemistry models and includes dust, sulfur, and smoke simulations. The Coupled Ocean-Atmosphere Mesoscale Prediction System (COAMPS) is a regional model that works in conjunction with NAAPS and provides the vertical distribution of aerosol particles [9]. Presently, however, NAAPS and COAMPS have not been applied to specific near-surface scenarios of interest for HEL applications.

The Navy Aerosol Model (NAM) [17,18] and its successor, the Advanced Navy Aerosol Model (ANAM) [12] are used to model near-surface maritime environments. While ANAM has been benchmarked in near-surface open-ocean conditions, it may not accurately represent the detailed composition and distribution of aerosols in regions where dust aerosols are expected to be present [9]. Nevertheless, ANAM can generate reasonable gross scattering and absorption coefficients which are sufficient for our purposes of simulating aerosol induced thermal blooming and laser scattering. In this study, we will use ANAM to generate the maritime aerosol scattering and absorption coefficients used in our simulations.

The "Navy Maritime" aerosol model of the MODTRAN atmospheric transmission code [19] uses NAM, but neglects the dust contribution, i.e., mode 0. Thus, it cannot be used to accurately describe near-shore maritime environments. The default MODTRAN "Maritime" aerosol model, however, gives aerosol absorption coefficients ($\sim 10^{-3}$ km^{-1}) that are similar to ANAM results for polluted coastal environments.

Mode	Material	R_{A0} [μm]	Re(n)	Im(n)
0	Non-hygroscopic dust	0.03	1.52	8×10^{-3}
1	Water soluable + water	0.03	1.37	9.6×10^{-5}
2	Sea salt + water ("aged" aerosol)	0.24	1.38	6.9×10^{-5}
3	Sea salt + water (new aerosol)	2	1.37	6.5×10^{-5}
4	Sea salt + water (near-surface)	8	1.37	6.5×10^{-5}

Table 3: Aerosol material composition, mean radius, and refractive index of the various ANAM aerosol modes for RH = 80%, $U_{10} = U_{24} = 5$ m/sec, AMP = 8, h = 5 m, $\lambda = 1.045\,\mu m$.

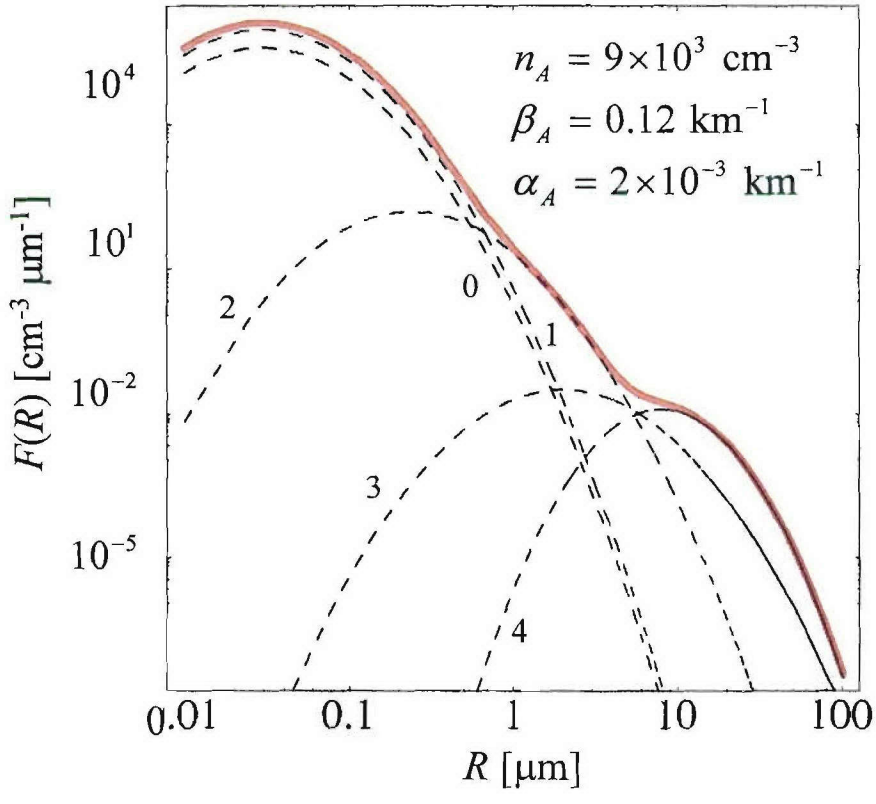

Figure 2: Aerosol distribution function calculated according to ANAM 3.0. Dashed curves denote individual aerosol modes 0-4. Solid curve denotes the total aerosol distribution function. RH = 80%, $U_{10} = U_{24} = 5$ m/sec, AMP = 8, h = 5 m, $\lambda = 1.045\,\mu m$.

The ANAM aerosol distribution is comprised of various modes which represent aerosols of different compositions and sizes. These aerosol modes will absorb laser energy and vaporize at different rates. The aerosol size distribution function, $F(R) = \sum_{j=0}^{4} F_j(R)$, where R is the aerosol radius, is represented as a superposition of five "modes" with each mode representing aerosols with a particular physical composition and origin. The total aerosol density is given by $n_A = \int dR\, F(R)$. Mode 0 represents dust particles of continental origin, mode 1 represents water-soluble aerosols, and modes 2-4 represent marine aerosols (sea salt and water) that result from different processes. NAM contains only modes 0 - 3. The physical properties of the various modes are summarized in Table 3. Each mode is described by a lognormal distribution over aerosol radius with a characteristic amplitude and width. The mean radius and distribution width of the water-based modes (1-4) are related to the ambient relative humidity (RH) using the model of Gerber [20]. The amplitude of modes 2 and 3 are related to the 24 hour averaged wind speed (U_{24}) and instantaneous wind speed at 10m altitude (U_{10}), respectively. The amplitude of mode 4 is related to the height above the sea surface (h) through an empirically determined relation. The air mass parameter (AMP) controls the amplitudes of modes 0 and 1. AMP is a dimensionless parameter varying between 1 (open ocean) and 10 (highly polluted coastal area) that qualitatively characterizes the amount of dust or continental aerosols in the atmosphere. However, it is not directly related to any measured meteorological parameter and can be varied somewhat arbitrarily to produce scattering coefficients that agree with measurements. As such, ANAM has no real predictive capability in regions where dusty aerosols are expected to play an important role. Figure 2 plots the ANAM aerosol distribution function for the various modes for RH = 80%, $U_{10} = U_{24} = 5$ m/sec, AMP = 8, and h = 5 m.

Calculation of the aerosol scattering and absorption coefficients also requires that the complex refractive index of the various aerosol modes and the complex cross section of the aerosol droplets, $\sigma = \sigma_{scat} + i\sigma_{abs}$, be known. Here, we take the refractive index

Maritime Environment (ANAM)			
Mode	Density [cm^{-3}]	β_A [km^{-1}]	α_A [km^{-1}]
0	2.6×10^{3}	0.028	1.6×10^{-3}
1	6.1×10^{3}	0.038	4.2×10^{-5}
2	9.0	0.032	3.2×10^{-5}
3	0.014	2.9×10^{-3}	2.4×10^{-5}
4	0.014	0.016	2.2×10^{-4}
Total	9×10^{3}	0.12	2×10^{-3}

Table 4: Aerosol number density, n_A, scattering coefficient, β_A, and volumetric absorption coefficient, α_A, associated with the various ANAM aerosol modes for the same parameters as used for Fig. 2, i.e., RH = 80%, $U_{10} = U_{24} = 5$ m/sec, AMP = 8, h = 5 m, $\lambda = 1.045 \mu m$.

of dust from Shettle and Fenn [21], sea salt and water-soluble materials are taken from from Volz [22, 23], and pure water from Hale and Query [24]. These indices are also tabulated in the technical documentation for NAM [18]. For modes 1-4 (hygroscopic aerosols) the refractive index is also a function of relative humidity. The values for n given in Table 3 are calculated for RH = 80 % [18]. The complex cross sections are calculated according to Mie theory. We use MODTRAN to calculate the molecular absorption and scattering coefficients [19].

Since the aerosol distribution can evolve with time, due to vaporization for example, the aerosol absorption and scattering coefficients are also time-dependent and given by

$$\alpha_A(t) = \int \sum_{j=0}^{4} \sigma_{abs,j}(R) F_j(R,t)\, dR, \tag{9a}$$

$$\beta_A(t) = \int \sum_{j=0}^{4} \sigma_{scat,j}(R) F_j(R,t)\, dR, \tag{9b}$$

where the scattering and absorption cross sections are $\sigma_{scat,j} = \pi R^2 Q_{scat,j}$ and $\sigma_{abs,j} = \pi R^2 Q_{abs,j}$, respectively, Q is the efficiency and j denotes mode number.

Table 4 lists the aerosol number density and scattering and absorption coefficients associated with each aerosol mode for the same parameters used in Fig. 2. For these parameters, mode 1 (water-soluble aerosols) has the largest number density. However, mode 0 has the largest absorption coefficient by far due to the large imaginary refractive index of dust-like aerosols. Mode 2 has the largest contribution to scattering. The total aerosol number density, scattering coefficient, and absorption coefficient associated with the distribution of Fig. 2 are given in Table 2, $n_A = 9 \times 10^3$ cm^{-3}, $\beta_A = 0.12$ km^{-1}, and $\alpha_A = 1.9 \times 10^{-3}$ km^{-1}, respectively. The corresponding visibility in this example is $\sim 3.9/\beta_A \sim 32$ km.

IV. Aerosol Heating and Vaporization

Scattering and blooming effects of aerosols can be reduced by vaporizing the water-based aerosols. The aerosol scattering and absorption coefficients are, in general,

functions of the size parameter $2\pi R_A / \lambda$. The aerosol absorption and scattering coefficient scales with aerosol radius as,

$$\alpha_A(t) \sim R_A^3(t), \tag{10a}$$

$$\beta_A(t) \sim \begin{cases} R_A^6(t), \text{ Rayleigh limit,} \\ \\ R_A^2(t), \text{ Mie limit,} \end{cases} \tag{10b}$$

where the Rayleigh and Mie limits are defined as $2\pi R_A / \lambda << 1$ and $2\pi R_A / \lambda >> 1$, respectively. Given the strong dependence of α_A and β_A on the aerosol radius, vaporization can reduce both the aerosol absorption and scattering coefficients. In the following we discuss the heating and vaporization of a single water-based aerosol droplet. We use these results to model the vaporization of a distribution of aerosols and the effect of vaporization on the atmospheric scattering and absorption coefficients.

i) Vaporization of an Aerosol Droplet

Heating and vaporization of a single water-based aerosol droplet are described by the following coupled equations for the aerosol temperature and radius [6],

$$\frac{\partial \Delta T_A}{\partial t} \approx \frac{\alpha_D I}{\rho_A c_A} + \frac{3 H_{vap}}{c_A R_A} \frac{\partial R_A}{\partial t} - \frac{3\kappa}{\rho_A c_A R_A^2} \Delta T_A, \tag{11a}$$

$$\frac{\partial R_A}{\partial t} \approx -\frac{\alpha_s \Lambda}{R_A} \Delta T_A, \tag{11b}$$

where $\Delta T_A = T_A - T_{amb}$, T_A is the aerosol temperature, T_{amb} is the ambient air temperature, R_A is the aerosol radius, $\alpha_D = \pi R_A^2 Q_{abs} / (4\pi R_A^3 / 3) = 3 Q_{abs} / 4 R_A$ is the bulk absorption coefficient of the aerosol droplet, $Q_{abs}(R)$ is the absorption efficiency, α_s is the evaporation coefficient (sticking fraction), ρ_A is the mass density of the droplet, κ is the thermal conductivity of air, c_A is the specific heat of the aerosol droplet, H_{vap} is the enthalpy of vaporization, $\Lambda = m_v D p_o \beta \exp(-\beta) / \rho_A k_B T_{amb}^2$, $\beta = M_{vap} H_{vap} / R T_{amb}$, m_v is the weight of a vapor molecule, $D = 0.24\,\text{cm}^2/\text{sec}$ is the

diffusion coefficient of air, k_B is the Boltzman constant, M_{vap} is the molecular vapor mass (e.g., $M_{vap} = 18$ for water vapor), $R = 8.3$ J/(K - mol) is the universal gas constant and p_0 is the constant of integration (with units of pressure) in the Clausius-Clapeyron formula, evaluated here for a saturated (i.e., 100% RH) water vapor pressure of 2.34 kPa at the temperature of 293 K. The first term on the right hand side of Eq. (11a) represents the absorbed laser energy, the second term is due to vaporization and the third is due to thermal conduction into the surrounding air. The rate of change of the aerosol radius is given by Eq. (11b). Equations (11a) and (11b) are valid for $\beta \Delta T_A / T_A << 1$ and $\tau_{vap} \equiv \left| \partial \ln R_A / \partial t \right|^{-1} >> R_A^2 \rho_A c_A / \kappa$. For water at $T_{amb} = 293\,\mathrm{K}$, $c_A = 4.2$ J/(g – K), $\kappa = 2.5 \times 10^{-4}$ W/(cm - K), $H_{vap} = 2.3\,\mathrm{kJ/g}$ and we find that $\beta = 17$, $\Lambda = 2.4 \times 10^{-7}$ cm^2/(K – sec). For a water-based aerosol with $R_A = 1$ μm, Eqs.(11a) and (11b) are valid for vaporization times $\tau_{vap} >> 0.1$ msec. The bulk absorption coefficient for an oceanic aerosol droplet is $\alpha_D = 8.4$, 30 and 59 cm^{-1} at the wavelengths $\lambda = 1.045\,\mu\mathrm{m}$, $1.625\,\mu\mathrm{m}$, and $2.141\,\mu\mathrm{m}$, respectively. Convection of the aerosols across the laser beam due to a wind or slew limits the heating and vaporization time to the local clearing time. This effect is contained in the full-scale numerical simulations of Sec. VI.

The aerosol temperature increases due to the absorbed laser energy and cools due to vaporization and thermal conduction. In the adiabatic regime, where the heating and cooling terms on the right hand side of Eq. (11a) are balanced, the aerosol temperature is given by

$$\Delta T_A = \frac{\alpha_D I R_A^2}{3\kappa(1+\eta)}, \tag{12}$$

where $\eta = \alpha_s H_{vap} \rho_A \Lambda / \kappa$ is the ratio of the aerosol vaporization energy to the aerosol energy conducted into the air; i.e., ratio of the last terms in Eq.(11a) [5]. For water at an ambient temperature of $T_{amb} = 293\,K$, it is found that $\eta = 2.2$. The adiabatic regime is reached in a time on the order of the thermal conduction time given by $\tau_{diff} = \rho_A c_A R_A^2 / \left(3\kappa(1+\eta)\right)$. For an aerosol with $R_A = 1$ μm, the thermal conduction

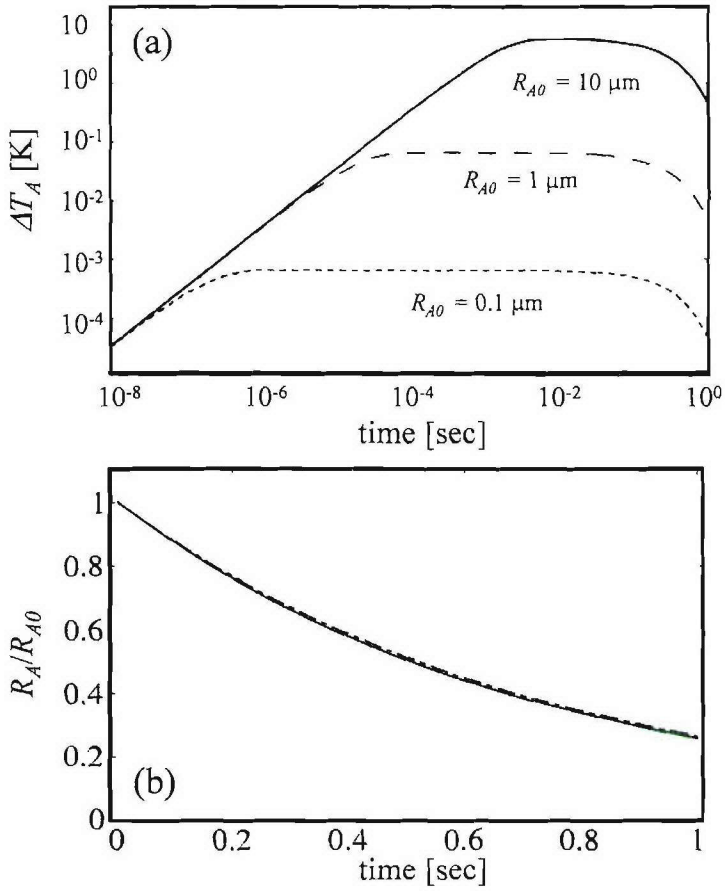

Figure 3: Aerosol temperature (a) and normalized radius (b) versus time for initial radii, R_{A0} = 0.1, 1, and 10 μm, and $\alpha_D I = 14$ kW/cm^3. Curves are almost indistinguishable in figure (b).

time is $\tau_{diff} \approx 20$ μsec. In the adiabatic limit and constant laser intensity the aerosol radius decreases exponentially with time according to

$$R_A(t) = R_{A0} \exp(-t/\tau_{vap}), \tag{13}$$

where R_{A0} is the initial radius of the aerosol and $\tau_{vap} = 3\rho_A H_{vap}(1+\eta^{-1})/(\alpha_D I)$ is the vaporization time.

Figure 3 plots the aerosol temperature and aerosol radius as a function of time as given by Eqs. (11a) and (11b). The laser intensity is taken to be $I = 2$ kW/cm^2. Figure (3a) shows that the temperature increases for a time comparable with the thermal conduction time before reaching a maximum value which is well-approximated by Eq. (12). Figure (3b) shows the characteristic exponential decrease of the aerosol radius in time. Note that for these parameters the vaporization time is essentially independent of initial radius, as predicted by Eq. (13).

ii) Vaporization of a Distribution of Aerosols

Assuming that the radius of each individual aerosol particle undergoing vaporization evolves according to $R_A(t) = R_{A0}\, h(t)$, as in Eq. (13), it can be shown that the aerosol radius distribution function can be written as

$$F(R,t) = \frac{F_0(R/h(t))}{h(t)}, \tag{14}$$

where $F_0(R)$ is the initial distribution function. In the adiabatic limit described by Eq. (14), each mode is characterized by $h_j(t) = \exp(-t/\tau_{vap,j})$, where $\tau_{vap,J} = 3\rho_{A,j} H_{vap,j}(1+\eta_j^{-1})/(\alpha_{D,j} I)$, for $j = 1$ to 4. We assume that mode 0 (non-hygroscopic dust) does not vaporize. In general, α_D is weakly dependent on the particle radius. However, for the purpose of obtaining a vaporization time for each mode, we take $\alpha_{D,J} = 4\pi\,\mathrm{Im}(n_j)/\lambda$, which is the absorption coefficient in the Rayleigh limit where n_j is the refractive index for aerosol mode j. For a constant laser intensity of

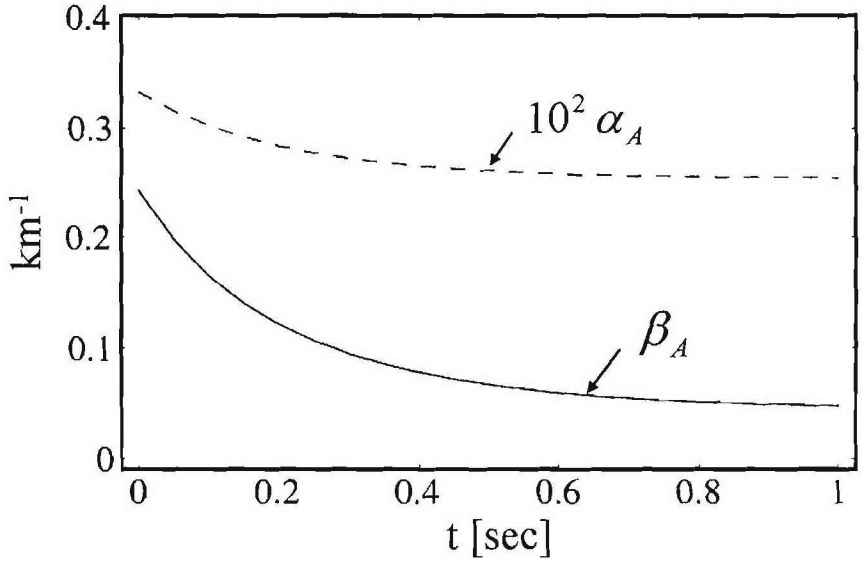

Figure 4: Aerosol absorption (dashed curve) and scattering coefficient (solid curve) for a distribution of aerosols versus time for a constant laser intensity, $I = 2$ kW/cm^2. The initial aerosol distribution corresponds to that of Fig. 2.

$I = 2$ kW/cm^2, the vaporization times associated with each mode are $\tau_{vap,1} = 0.42$ sec, and $\tau_{vap,2} = \tau_{vap,3} = \tau_{vap,4} \approx 0.62$ sec.

Figure 4 plots the total aerosol scattering and absorption coefficients versus time. The scattering coefficient is seen to decrease by a factor of 5 after ~ 1 sec. The absorption coefficient is not decreased significantly due to the presence of non-hygroscopic aerosols (mode 0) which do not vaporize.

V. Thermal Blooming in the Presence of Aerosols

Propagation of a high energy laser beam in the atmosphere results in a small fraction of the laser energy being absorbed by both the molecular and aerosol constituents of air. The absorbed energy locally heats the air and leads to a decrease in the air density which modifies the refractive index, given by $\delta n_{TB} = (n_0 - 1)\delta\rho / \rho_0$, where ρ_0 and $\delta\rho$ are the ambient and perturbed air mass densities, respectively. The refractive index variation leads to a defocusing or spreading of the laser beam known as thermal blooming [1].

For an isobaric process the perturbed air temperature δT is related to the perturbed density by $\delta\rho = -(\rho_o / T_o)\delta T$ and evolves in time according to

$$c_p \rho_o \left(\frac{\partial}{\partial t} + \mathbf{V}_W \cdot \nabla - \frac{\kappa}{c_p \rho_o} \nabla^2 \right) \delta T = \alpha_{total} I, \qquad (15)$$

where κ is the thermal conductivity, c_p is the specific heat of air at constant pressure, $\mathbf{V}_W$ is the wind or slew velocity and I is the time-averaged laser intensity. The isobaric regime is valid for times greater than the hydrodynamic time R_L / C_s, where R_L is the laser spot size and C_s is the acoustic speed.

The rate of change of laser energy density absorbed in air determines the degree of thermal blooming and is given by the total absorption coefficient α_{total},

$$\alpha_{total} I = \alpha_{WV} I + 4\pi\kappa n_A R_A \Delta T_A + \alpha_{WV} \frac{\rho_{WV}}{\rho_{WV,amb}} I + \frac{2\pi n_A \rho_A k_B \Delta T_A}{m_v} \frac{\partial R_A^3}{\partial t}, \qquad (16)$$

where the first term on the right hand side is due to ambient water vapor absorption, the second is due to conductive heating of the air from the heated aerosols, the third is due to the additional water vapor from the vaporized aerosols, and the last term is due to the fact that water vapor from a vaporized aerosol enters the air at an elevated temperature. The third term is small compared to the first since $\rho_{WV} / \rho_{WV,amb} << 1$, and the ratio of the fourth to the second term is

$$\frac{3\rho_A k_B R_A}{2 m_v \kappa} \frac{\partial R_A}{\partial t} = 0.2\alpha_s \Delta T_A / T_{amb} << 1.$$

Hence, the last two terms on the right side of Eq. (16) can be neglected.

A further simplification applies in the adiabatic regime where the temperature change is proportional to the laser intensity. Substituting Eq. (12) for ΔT_A into Eq. (16) results in the following thermal blooming absorption coefficient for a homogeneous aerosol distribution

$$\alpha_{\text{total}} = \alpha_{WV} + \frac{\alpha_D n_A}{1+\eta}\left(\frac{4\pi R_A^3}{3}\right). \tag{17}$$

The result in Eq.(17) is important because it shows that aerosol absorption, modified by vaporization, contributes directly to the thermal blooming absorption coefficient.

In general, for a non-homogeneous aerosol distribution, the last term in Eq.(17) must be averaged over the aerosol distribution to give $\alpha_{\text{total}} = \alpha_{WV} + \alpha_A/(1+\eta)$, where we have used the definition of the aerosol absorption coefficient, $\alpha_A \equiv \int F(R) Q_{abs}(R) \pi R^2 dR$ where $Q_{abs}(R) = 4R\alpha_D(R)/3$ is the imaginary part of the scattering efficiency. For the multi-mode aerosol distribution of Fig. 2, Eq. (17) can be written as

$$\alpha_{total} = \alpha_{WV} + \sum_{j=0}^{4} \frac{\alpha_{A,j}}{1+\eta_j}. \tag{18}$$

The aerosol contribution to the overall absorption coefficient can be much larger than that of molecular water vapor. For example, in the "water window" at wavelength 1.045μm, $\alpha_{WV} = 3\times10^{-5}$ km^{-1}, while from Table 4 the effective aerosol contribution

can be up to two orders of magnitude larger. When non-hygroscopic aerosols represent a large fraction of the aerosol population, it is not possible to significantly reduce the absorption coefficient by vaporization. Therefore, the optimum laser wavelength for reducing thermal blooming should not be primarily determined by the transmission windows of molecular water vapor, but must also consider the absorption and conductive air heating due to aerosols.

VI. Simulations of HEL Propagation

In this section we present results of full-scale computer simulations of HEL propagation through various atmospheric environments. The propagation code used for this study is HELCAP (High Energy Laser Code for Atmospheric Propagation) which is a fully time-dependent, 3D code developed at the Naval Research Laboratory [15]. HELCAP models the propagation of continuous and pulsed HELs through the atmosphere. Representing the laser electric field as $\mathbf{E} = A(x,y,z,t)\exp[\, i(\omega_o z/c - \omega_o t)]\, \hat{\mathbf{e}}_x/2 + c.c.$, where $\omega_o = 2\pi c/\lambda$ is the laser frequency, $\hat{\mathbf{e}}_x$ is a unit polarization vector in the x direction, $A(x,y,z,t)$ is the complex laser amplitude and the laser intensity is $I = c\,A\,A^*/8\pi$. HELCAP solves a nonlinear Schrödinger-like equation which has the form

$$\frac{\partial A}{\partial z} = \frac{ic}{2\omega_o}\nabla_\perp^2 A + \left[i\frac{\omega_o}{c}(\delta n_T + \delta n_{TB}) - \frac{1}{2}(\alpha + \beta)\right] A + \sum_j S_j\,, \qquad (19)$$

where $\alpha = \alpha_m + \alpha_A$ is the total absorption coefficient, $\beta = \beta_m + \beta_A$ is the total scattering coefficient, and δn_T and δn_{TB} denote the refractive index variation due to atmospheric turbulence and thermal blooming respectively. $\alpha_m\,(\alpha_A)$ is the molecular (aerosol) absorption coefficient. $\beta_m\,(\beta_A)$ is the molecular (aerosol) scattering coefficient. The quantities δn_T, δn_{TB}, α, and β are space and time-dependent and determined self-consistently in the presence of the effects discussed in the previous sections, e.g., aerosol heating and vaporization. The effects of wind or beam slew, on the air and aerosol heating is contained in the full scale simulations presented in this Section.

The terms denoted by $\sum_j S_j$ represent other physical processes such as group velocity dispersion, ionization, relativistic effects, nonlinear Kerr effects, and stimulated Raman scattering. While these processes do not significantly affect the propagation of the HEL beams considered here, they are important for the propagation of ultra-high intensity femtosecond laser pulses [25, 26].

In the following examples, we consider the propagation of HEL beams in i) maritime, ii) desert, iii) rural, and iv) urban atmospheres. In these examples, the laser wavelengths are taken to be 1.045 μm, 1.625 μm, and 2.141 μm, which correspond to atmospheric transmission windows, i.e., minima in molecular (water vapor) absorption. HELCAP requires the initial scattering and absorption coefficients associated with vaporizable (water-based) and non-vaporizable (e.g., dust, soot) aerosol constituents as inputs. For the maritime atmosphere we use ANAM to generate the aerosol scattering and absorption coefficients. For the urban, rural, and desert environments we use MODTRAN4 and the Air Force Geophysics Laboratory (AFGL) model of Ref. [27] to generate the aerosol parameters. MODTRAN4 yields the overall aerosol scattering and absorption coefficients while the AFGL model gives the physical compositions and percentages of vaporizable and non-vaporizable aerosols.

The propagation configuration is shown in Fig.1. The high energy laser beam has an initial field profile given by $A = A_0 f(r)\, g(t) \exp(-r^2 / R_0^2)$, where $f(r) = \exp[-(2r/D)^{\ell}]$, $\ell = 20$, limits the transverse extent of the beam to the aperture diameter, D, and $g(t)$ is the initial temporal profile of the beam. The transmitted power at the source is denoted by P_T. The laser is focused onto a remote target at a range of 5 km. The target is taken to be circular with an area of 100 cm^2. The propagation direction is along the z-axis and a uniform transverse wind, with velocity V_w = 5 m/sec is directed along the y-axis. Atmospheric turbulence is modeled by a Kolmogorov spectrum with structure constant $C_n^2 = 10^{-15}$ $m^{-2/3}$. The pointing jitter associated with the laser beam is taken to have an angular spread of 2 μrad and a white noise temporal spectrum. Since thermal blooming and turbulence can cause the laser beam centroid to wander, adaptive optics techniques are employed to keep the laser beam centered on the target. In the

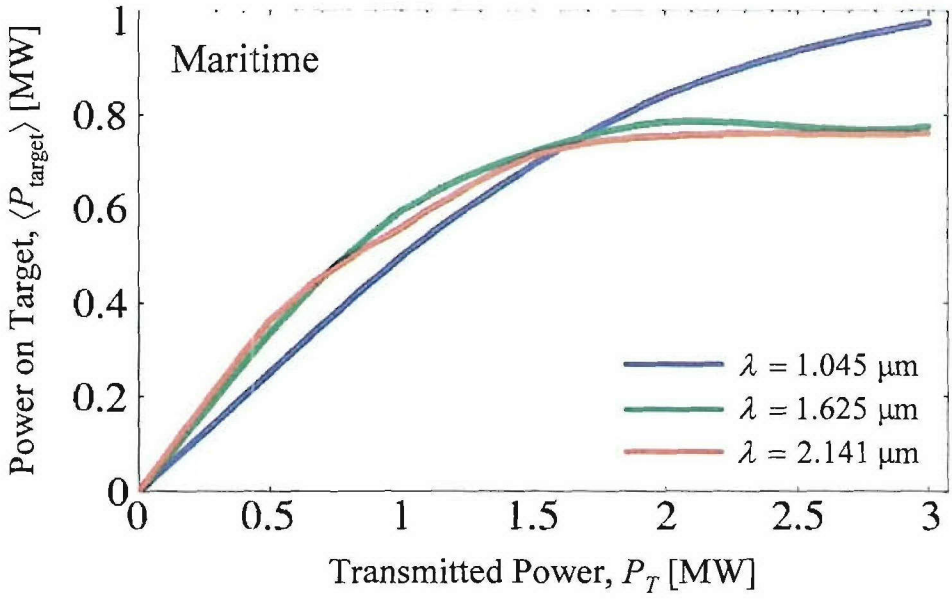

Figure 5: Average power on target, $\langle P_{target} \rangle$, versus transmitted power, P_T, in a maritime environment for the wavelengths λ = 1.045, 1.625, 2.141 μm. Initial beam profile has R_0 = 50 cm, D = 80 cm. Simulation geometry is shown in Fig. 1. Aerosol properties are listed in Table 4. Target range, L = 5 km; beam focus = 5 km; target area = 100 cm^2; wind speed, V_w = 5 m/sec; turbulence strength, $C_n^2 = 10^{-15}$ m$^{-2/3}$; pointing jitter angular amplitude = 2 μrad (white noise).

simulations, the target is always located such that the peak laser fluence at 5 km range is at the center of the target.

The average power on target is used as a figure of merit in the following examples. It is defined by

$$\left\langle P_{\text{target}} \right\rangle = \frac{1}{\tau_{dwell}} \int_0^{\tau_{dwell}} d\tau \int dx dy \, I(x, y, z = L, \tau), \tag{20}$$

where the dwell time $\tau_{dwell} = 1$ sec, and $dx\,dy$ is the differential cross section which is integrated over the target area. The total laser energy reaching the target is $E_{\text{target}} = \left\langle P_{\text{target}} \right\rangle \tau_{dwell}$. However, this laser energy is not necessarily absorbed by the target. Calculation of the absorbed laser energy requires additional information such as the target material absorption coefficient, surface roughness, surface curvature, etc, which is not considered here.

i) Maritime Environment

The maritime environment is characterized by a mixture of salt water aerosols, water soluble aerosols and dust aerosols, as described in Sec. III. In this example we use the aerosol distribution shown in Fig. 2 to calculate the scattering and absorption coefficients. These coefficients, as well as the molecular absorption coefficients, are listed in Table 1. For the vaporization calculations, we assume droplet absorption coefficient of $\alpha_D = 8\ \text{cm}^{-1}$, $30\ \text{cm}^{-1}$, and $59\ \text{cm}^{-1}$ for the wavelength $\lambda = 1.045\ \mu\text{m}$, $1.625\ \mu\text{m}$, and $2.141\ \mu\text{m}$, respectively. These values are calculated assuming 80% RH and using the refractive index for oceanic aerosols [18].

Figure 5 plots the average power on target versus the transmitted power, P_T, for the three wavelengths of interest. Our results show that for a maritime environment, the optimum wavelength depends on the transmitted power. For $P_T < 1.5$ MW, propagation is mostly affected by aerosol scattering and the average power on target increases with P_T. In this regime, the $1.625\ \mu\text{m}$, and $2.141\ \mu\text{m}$ wavelengths provide slightly greater power on target than $1.045\ \mu\text{m}$. This is due to the lower aerosol scattering coefficient associated with the longer wavelengths. For $P_T < 1$ MW, the propagation efficiency is

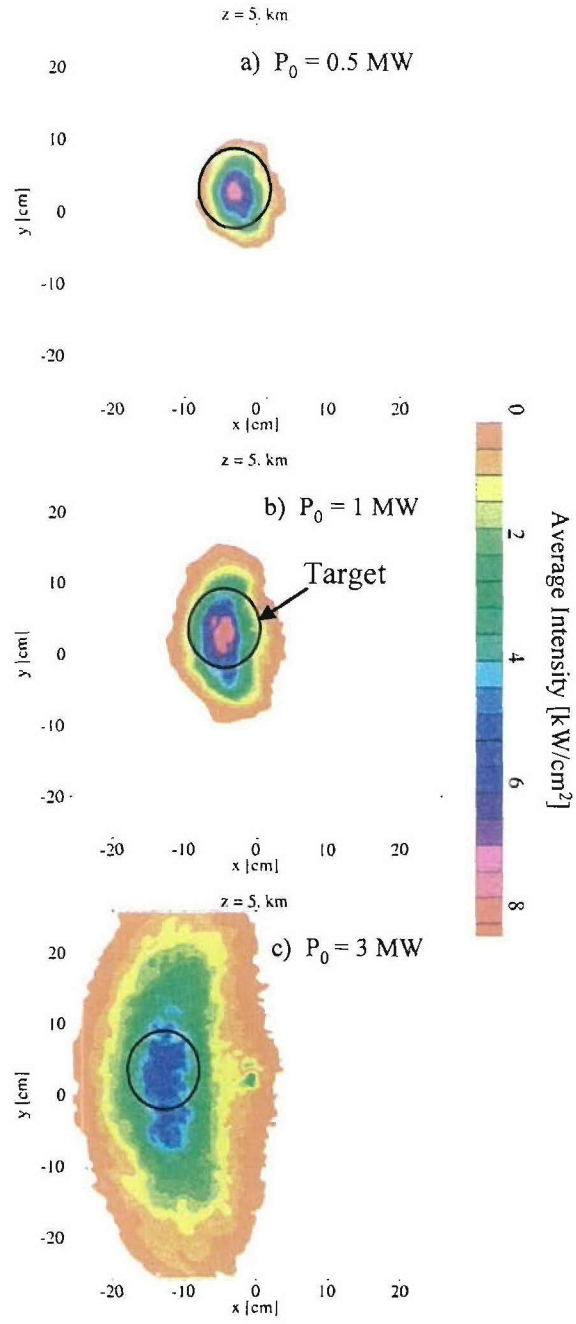

Figure 6: Time-averaged intensity in the target plane for transmitted powers, a) P_T = 0.5 MW, b) P_T = 1 MW, and c) P_T = 3 MW, and λ = 1.625 μm. Time average is done over 1 sec dwell time. Parameters correspond to those of Fig. 5.

Roughly 50% for the three wavelengths considered. For example, P_T = 1 MW results in $\langle P_{\text{target}} \rangle \sim 0.55$ MW for $\lambda = 1.625\,\mu\text{m}$ and $\lambda = 2.141\,\mu\text{m}$. However, for $P_T > 1.5$ MW, thermal blooming becomes important. In this high power regime the optimum wavelength is 1.045 μm due to the lower molecular absorption coefficient in that water vapor window. For $P_T = 3$ MW, $\langle P_{\text{target}} \rangle \sim 1$ MW for 1.045 μm while $\langle P_{\text{target}} \rangle \sim 0.8$ MW for 1.625 μm and 2.141 μm.

The effect of thermal blooming on the laser spot size on target is shown in Fig. 6. Figure 6 shows contours of the time averaged intensity in the target plane for three values of transmitted power at $\lambda = 1.625$ μm. The time average is performed over the entire dwell time of 1 sec. The laser spot size on target is seen to increase with increasing P_T. For relatively low power, $P_T = 0.5\,\text{MW}$, the beam is focused within the 100 cm^2 target area and the loss of power on the target is mainly due to aerosol scattering. When $P_T = 1\,\text{MW}$, the laser beam extends slightly beyond the target area. For $P_T = 3\,\text{MW}$, the beam cross section is much larger than the target area and exhibits a crescent shape characteristic of thermal blooming in the presence of a wind. In these simulations, aerosol vaporization effects increased the average power on target by ~ 10% for $P_T \geq 1.5\,\text{MW}$.

ii) Desert Environment

The desert aerosol environment is characterized by dry, dust-like aerosols which cannot be vaporized at the laser intensities considered here. These aerosols absorb laser energy, heat the surrounding air and significantly contribute to thermal blooming. The aerosol absorption and scattering coefficients, generated using the MODTRAN4 desert model with a 10 km visibility, are shown in Table 5 for the three wavelengths of interest. The molecular absorption coefficients are taken to be the same as in the maritime environment.

Figure 7 plots the average power on target versus transmitted power, P_T, for the three wavelengths of interest. The results are qualitatively similar to those of the maritime environment, i.e., the optimum wavelengths are 1.625 μm and 2.141 μm for

Desert Environment		
λ [μm]	α_A [km^{-1}]	β_A [km^{-1}]
1.045	7×10^{-4}	0.17
1.625	5×10^{-4}	0.097
2.141	6×10^{-4}	0.072

Table 5: Aerosol absorption (α_A) and scattering (β_A) coefficients at wavelengths λ = 1.045, 1.625, 2.141 μm for a model desert environment generated using MODTRAN4, 10 km visibility.

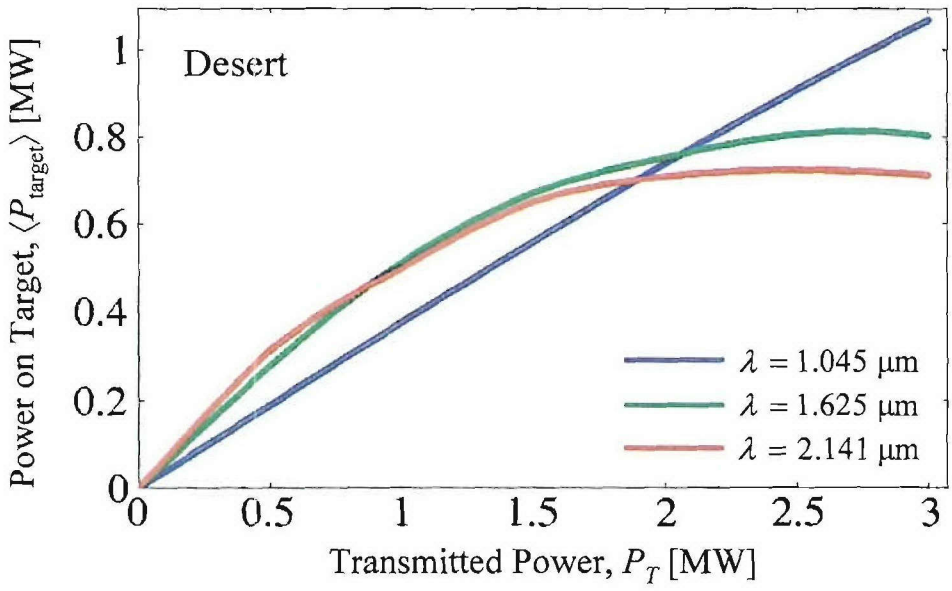

Figure 7: Average power on target, $\langle P_{target} \rangle$, versus transmitted power, P_T, in a desert environment for the wavelengths λ = 1.045, 1.625, 2.141 μm. Initial beam profile has R_0 = 50 cm, D = 80 cm. Simulation geometry is shown in Fig. 1. Aerosol properties are listed in Table 5. Target range, L = 5 km; beam focus = 5 km; target area = 100 cm^2; wind speed, V_W = 5 m/sec; turbulence strength, $C_n^2 = 10^{-15}$ m$^{-2/3}$; pointing jitter angular amplitude = 2 μrad (white noise).

$P_T < 2$ MW, and 1.045 μm for $P_T > 2$ MW. In a desert environment, $P_T = 1$ MW results in $\langle P_{\text{target}} \rangle \sim 0.5$ MW for 1.625 μm and 2.141 μm wavelengths, and $\langle P_{\text{target}} \rangle \sim 0.35$ MW for 1.045 μm. For $P_T = 3$ MW, $\langle P_{\text{target}} \rangle \sim 1.3$ MW for 1.045 μm , ~ 0.8 MW for 1.625 μm, and ~ 0.7 MW for 2.141 μm wavelengths.

iii) Rural Environment

The rural aerosol environment is taken to be a mixture of 70% water soluble aerosols and 30% dust-like aerosols [27]. The total aerosol absorption and scattering coefficients for the rural environment are shown in Table 6. These coefficients are generated using the MODTRAN4 rural model with a 10 km visibility. At the laser intensity levels considered, the dust-like aerosols are not vaporized while the water soluble aerosols are partially vaporized. In the vaporization calculations, the absorption coefficient of the aerosol droplet is taken to be $\alpha_D = 1.2 \times 10^3$ cm^{-1} , 1.0×10^3 cm^{-1}, and 3.5×10^2 cm^{-1} for the wavelengths $\lambda = 1.045$ μm , 1.625 μm , and 2.141 μm , respectively. These values are calculated using the refractive index for water soluble aerosols [27], assuming 80% RH.

Figure 8 plots the average power on target versus transmitted power for the rural environment. Because of the large absorption coefficient of the water soluble and dust aerosols thermal blooming begins to be a limiting process for $P_0 > 0.5$ MW. For the rural environment, 2.141 μm is the optimum wavelength over the entire range $P_T < 3$ MW. The optimum power for a wavelength of 2.141 μm is $P_T \sim 1.5$ MW which results in $\langle P_{\text{target}} \rangle \sim 0.6$ MW. For $P_T > 1.5$ MW, the power on target is limited by thermal blooming.

iv) Urban Environment

The aerosol absorption and scattering coefficients are generated using the MODTRAN4 urban aerosol model with a 10 km visibility. Table 7 lists the calculated scattering and absorption coefficients. The aerosol absorption in an urban environment is

Rural Environment		
λ [μm]	α_A [km^{-1}]	β_A [km^{-1}]
1.045	0.016	0.15
1.625	0.012	0.076
2.141	0.006	0.053

Table 6: Aerosol absorption (α_A) and scattering (β_A) coefficients at wavelengths λ = 1.045, 1.625, 2.141 μm for a model rural environment generated using MODTRAN4, 10 km visibility.

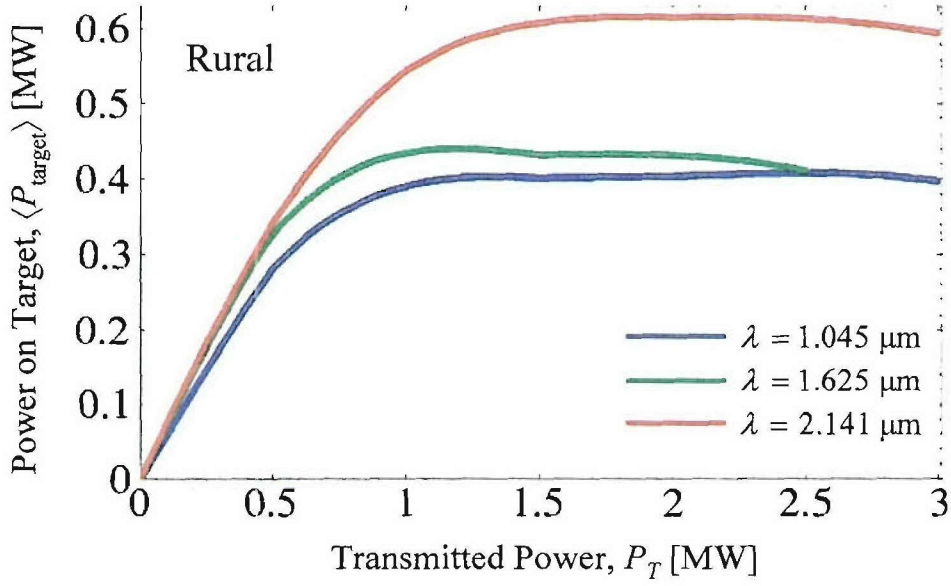

Figure 8: Average power on target, $\langle P_{\text{target}} \rangle$, versus transmitted power, P_T, in a rural environment for the wavelengths λ = 1.045, 1.625, 2.141 μm. Initial beam profile has R_0 = 50 cm, D = 80 cm. Simulation geometry is shown in Fig. 1. Aerosol properties are listed in Table 6. Target range, L = 5 km; beam focus = 5 km; target area = 100 cm^2; wind speed, V_W = 5 m/sec; turbulence strength, $C_n^2 = 10^{-15}$ m$^{-2/3}$; pointing jitter angular amplitude = 2 μrad (white noise).

Urban Environment		
λ [μm]	α_A [km^{-1}]	β_A [km^{-1}]
1.045	0.05	0.13
1.625	0.036	0.065
2.141	0.028	0.044

Table 7: Aerosol absorption (α_A) and scattering (β_A) coefficients at wavelengths λ = 1.045, 1.625, 2.141 μm for a model urban environment generated using MODTRAN4, 10 km visibility.

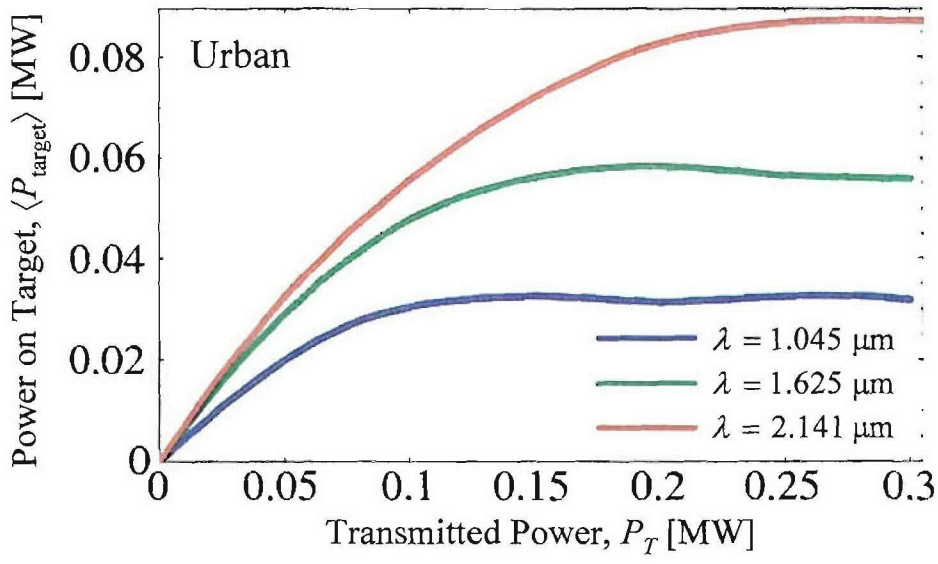

Figure 9: Average power on target, $\langle P_{\text{target}} \rangle$, versus transmitted power, P_T, in an urban environment for the wavelengths λ = 1.045, 1.625, 2.141 μm. Initial beam profile has R_0 = 50 cm, D = 80 cm. Simulation geometry is shown in Fig. 1. Aerosol properties are listed in Table 7. Target range, L = 5 km; beam focus = 5 km; target area = 100 cm^2; wind speed, V_W = 5 m/sec; turbulence strength, $C_n^2 = 10^{-15}$ m$^{-2/3}$; pointing jitter angular amplitude = 2 μrad (white noise).

the largest of the four environments considered. Urban aerosols are modeled as a mixture of 80% rural aerosols and 20% soot aerosols [27]. Soot aerosols, which cannot be vaporized, represent the dominant contribution to aerosol absorption. Hence they heat the air and cause significant thermal blooming of the laser.

Figure 9 plots the average power on target versus the transmitted power. For the urban environment, 2.141 μm is the optimum wavelength over the entire range $P_T < 3$ MW. The optimum transmitted power for the 2.141 μm wavelength is $P_T \sim 0.3$ MW, which results in a power on target of only $\langle P_{\text{target}} \rangle \sim 0.09$ MW.

v) Air-to-Ground Propagation in Desert and Urban Environments

Finally, we consider the propagation of a HEL beam from a high altitude fast-moving airborne platform or plane, to a stationary target on the ground. The plane is located at z = 0 and the target is at z = L = 5 km. The laser beam has an effective slew velocity of $V_w = V_0[1 - (z/L)]$, where $V_0 = 100$ m/sec is the plane velocity. The background wind velocity is zero. This configuration produces a stagnation zone near the ground, i.e., target. The turbulence strength, scattering coefficients, and absorption coefficients are assumed to vary with atmospheric density according to, for example, $C_n^2 = C_{n,g}^2 \exp[(z-L)/L_{atm}]$ where $C_{n,g}^2 = 10^{-15}$ $m^{-2/3}$ is the turbulence strength at ground level and $L_{atm} = 8$ km is the characteristic height scale for the atmospheric density. All other parameters are the same as in the previous examples. The range to the target is assumed to be constant.

Figure 10 plots the average power on target versus the transmitted power for a desert and urban environment. It is seen that in the desert environment the large slew effectively reduces thermal blooming and results in propagation efficiencies of greater than $\eta \approx 60\%$ for the case of the 2.141 μm wavelength laser. In the urban environment, thermal blooming is still a limiting factor due to the large absorption of soot aerosols. However, the propagation efficiency in this vertical propagation example is much greater than for the urban horizontal propagation example of Fig. 9. For the optimum wavelength of 2.141μm, the propagation efficiency at $P_T = 1$ MW is $\eta \approx 45\%$.

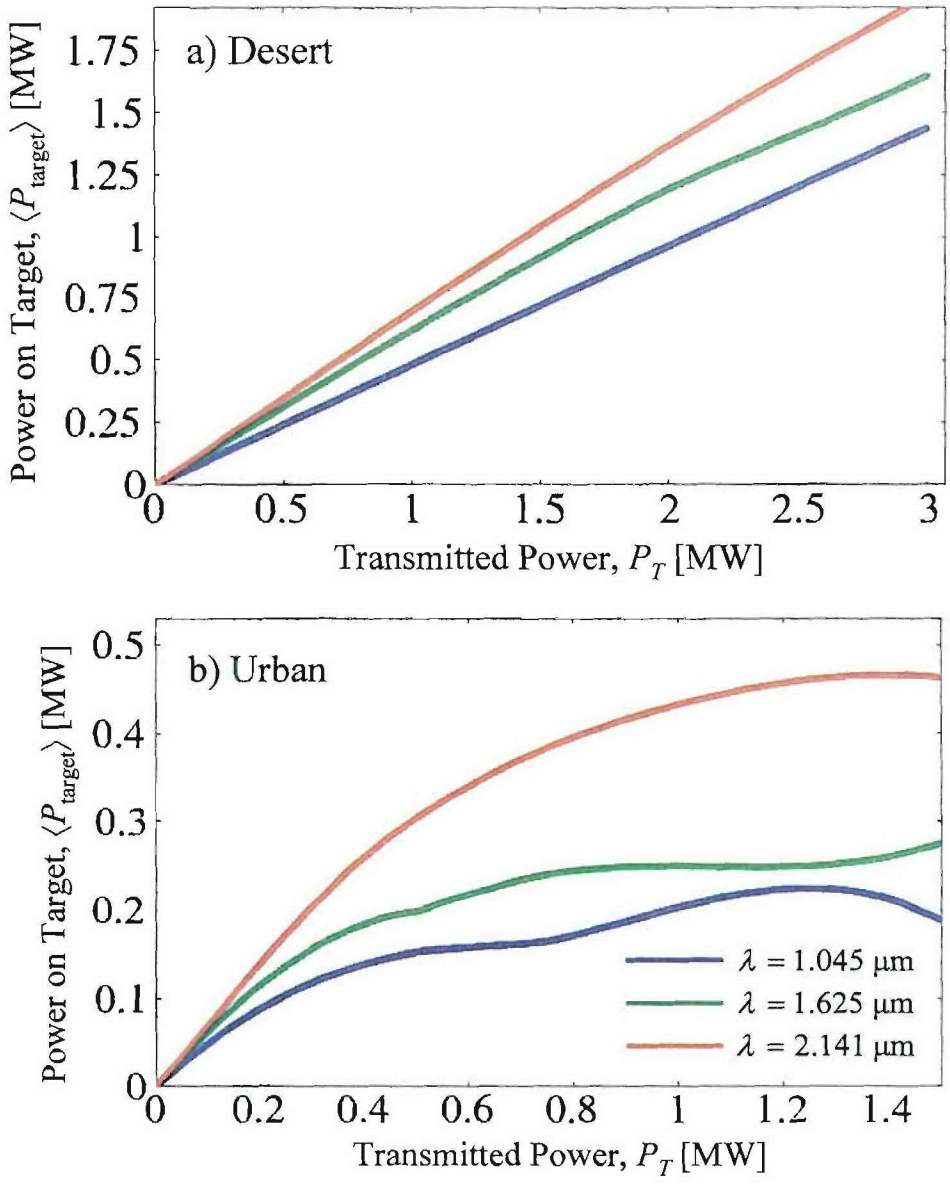

Figure 10: Average power on target, $\langle P_{target} \rangle$, versus transmitted power, P_T, in a a) desert environment and b) urban environment for the wavelengths λ = 1.045, 1.625, and 2.141 μm for vertical air-to-ground propagation. Initial beam profile has $R_0 = 50$ cm, $D = 80$ cm. Simulation geometry is shown in Fig. 1. Aerosol properties are listed in Tables 5 and 7. Target range, L = 5 km; beam focus = 5 km; target area = 100 cm^2; wind speed, $V_W = V_0[1 - (z/L)]$, V_W = 100 m/sec; turbulence strength, $C_n^2 = C_{n,g}^2 \exp[(z-L)/L_{atm}]$, $C_{n,g}^2 = 10^{-15}$ m$^{-2/3}$, L_{atm} = 8 km; pointing jitter angular amplitude = 2 μrad (white noise).

VII. Conclusions

In this paper we have analyzed the physical processes that affect the propagation of high energy laser (HEL) beams and employed HELCAP, a fully three-dimensional, time-dependent numerical simulation code, to determine the optimum laser wavelength and power for HEL propagation in maritime, desert, rural, and urban environments. The aerosol absorption and scattering coefficients which characterize these environments were generated using the ANAM and MODTRAN aerosol models.

The theoretical model and numerical simulations contain several interrelated physical processes which affect HEL propagation. These include: i) aerosol and molecular scattering ii) aerosol heating and vaporization iii) thermal blooming due to both aerosol and molecular absorption iv) atmospheric turbulence and v) laser beam quality. HELCAP is unique in that it contains all of these physical processes in a fully time-dependent and self-consistent manner.

Using HELCAP, we calculated the average power, $\langle P_{\text{target}} \rangle$, delivered to a 100 cm^2 cross sectional area target at a range of 5 km over a 1 second dwell time as a function of transmitted power, P_T, and wavelength. We considered three laser wavelengths corresponding to molecular (water vapor) transmission windows, 1.045 μm, 1.625 μm and 2.141 μm, and transmitted powers P_T up to 3 MW. We note that in addition to the power propagated to the target, $\langle P_{\text{target}} \rangle$, the absorption efficiency of the target should be considered in evaluating HEL lethality. Target absorption efficiency is relatively insensitive to wavelength in the range considered.

We find that aerosols are of particular importance because they result in laser scattering, absorption, and enhanced thermal blooming. In the water vapor transmission windows, the total absorption coefficient driving thermal blooming can be due mainly to aerosols and not to water vapor. In certain environments and for sufficiently high laser power, scattering and absorption by aerosols can be reduced by vaporization. Aerosols that consist of dust, soot, etc., cannot be vaporized and can significantly enhance thermal blooming. We note that moderate values of the laser beam quality factor M^2, i.e., values

less than 4, have little effect on the propagation of HELs compared to other effects such as, molecular/aerosol thermal blooming and turbulence.

Our results show that the average power on target is strongly dependent on the atmospheric environment:

Maritime: In a maritime environment, for $P_T < 1.5$ MW, the propagation efficiency varies from $\eta \approx 50\%$ to 70%. In this transmitted power range the 1.625 μm, and 2.141 μm wavelengths provide slightly greater efficiency than 1.045 μm. However, for $P_T > 1.5$ MW, thermal blooming limits the power on target. In this high power regime, the optimum wavelength is 1.045 μm due to stronger absorption at the other wavelengths (see Fig. 5).

Desert: The aerosols in a desert environment are composed mainly of dust particles, however, the gross extinction coefficients are similar to that of a maritime environment. Hence, the power on target for the desert environment is very similar to the maritime environment for $P_T < 1.5$ MW (see Fig. 7). At higher transmitted powers, however, there is slightly less thermal blooming for 1.045 μm compared to the maritime environment due to the relatively lower aerosol absorption in a desert environment.

Rural: For the rural environment 2.141 μm is the optimum wavelength over the entire range of transmitted powers, $P_T < 3\,\text{MW}$. The optimum power is found to be $P_T \sim 1.5$ MW which results in an average power of $\langle P_{\text{target}} \rangle \sim 0.6$ MW and efficiency of $\eta \approx 40\%$. For $P_T > 1.5$ MW, the power on target does not increase with transmitted power because of thermal blooming.

Urban: The optimum wavelength for the urban environment is found to be 2.141 μm over the entire range $P_T < 3$ MW (see Fig. 9). However, thermal blooming due to the non-hygroscopic aerosols places severe limits on the transmitted power. For example, the maximum value of $\langle P_{\text{target}} \rangle \sim 0.08$ MW is obtained for $P_T \sim 0.2$ MW, giving an efficiency of $\eta \approx 40\%$ (Fig.9).

Air to Ground (Desert, Urban): We have also considered vertical propagation scenarios from a fast moving platform to a stationary target on the ground in both a desert and urban environment. In these cases we find that for the desert environment, the large

beam slew negates thermal blooming effects and results in high propagation efficiency, $\eta > 60\%$ for $2.141\,\mu m$. In the urban environment, however, the presence of soot aerosols can still result in significant thermal blooming (see Fig. 10).

When the propagating efficiency is not a particularly sensitive function of wavelength, as in the maritime and desert environments for $P_T < 1.5$ MW, other issues such as laser availability and/or eye safe wavelengths, may become important considerations in determining the optimum wavelength and power. In this study we have reported only on wavelengths in the water vapor transmission windows, $\lambda = 1.045$, 1.625, and $2.141\,\mu m$. Other laser wavelengths, such as those particular to solid state and chemical lasers, have also been considered. In general, it is found that at high laser powers, for which thermal blooming is a factor, operating in the water vapor window results in higher propagating efficiencies.

Acknowledgments

The authors thank A. Ting, J. Albertine, J. Reid, S. Doss-Hammel and Q. Saulter for many useful discussions. This work was sponsored by the Joint Technology Office and the Office of Naval Research.

References

[1] Smith, D.C., "High-Power Laser Propagation - Thermal Blooming," Proc. IEEE 65, 1679 (1977)

[2] The Infrared and Electro-Optical Systems Handbook, vol. 2, edited by F.G. Smith, Environmental Research Institute of Michigan, Ann Arbor, MI, and SPIE Optical Engineering Press, Bellingham, WA (1993).

[3] Measures, R.M., "Laser Remote Sensing, Fundamentals and Applications," Krieger Publishing, Malabar, FL (1992)

[4] Williams, F. A, Int. J. Heat Mass Transfer. **8**, 575 (1965).

[5] Caledonia, G.E. and J.D. Teare, J. Heat Transfer **99**, 281 (1977).

[6] Armstrong, R.L., Appl. Optics **23**, 148 (1984); Armstrong, R.L., J. Appl. Phys. **56**, 2142 (1984); Armstrong, R.L., S.A.W. Gerstl and A. Zardecki, J. Opt. Soc. Am. A **2**, 1739 (1985).

[7] Davies, S.C. and J.R. Brock, App. Optics **26**, 786 (1987)

[8] Hänel, G., Beiträge zur Physik der Atmosphäre **44**, 137 (1971)

[9] Reid, J.S., D.L. Westphal, R.M. Paulus, S. Tsay and A. van Eijk, "Preliminary Evaluation of the Impacts of Aerosol Particles on Laser Performance in the Coastal Marine Boundary Layer," Naval Research Laboratory, Monterey, CA 93943-5502, NRL/MR/7534—04-8803, Jun. 2004.

[10] Brown R.T. and D.C. Smith, J. App. Phys. **46**, 402 (1975)

[11] Fulghum, S.F., and M.M. Tilleman, J. Opt. Soc. Am. B **8**, 2401 (1991)

[12] van Eijk, A.M.J. and L.H. Cohen, "The ANAM-3.0 Development," TNO Physics and Electronics Laboratory, Jun. 2005; Piazzola, J., M.J. van Eijk, G. de Leeuw, Opt. Eng. **39**, 1620 (2000).

[13] Doss-Hammel, S., D. Tsintikidis, D. Merritt and J. Fontana, "Atmospheric Characterization for High Energy Laser Beam Propagation in the maritime Environment," Proc. SPIE, vol. 5552, SPIE, Bellingham, WA, 2004, p. 208.

[14] Bodhaine, B.A., J. Geophys. Res. **100**, 8967 (1995)

[15] Sprangle, P., J. R. Penano, A. Ting, B. Hafizi and D.F. Gordon, Journal of Directed Energy 1, **73** (2003)

[16] Berger P.J., P.B. Ulrich, J.T. Ulrich, and F.G. Gebhardt, Applied Opt. **16**, 345 (1977)

[17] Gathman, S.G., Opt. Eng. **22**, 057 (1983) ; Gathman, S.G. and K.L. Davidson, "The Navy Oceanic Vertical Aerosol Model," Technical Report 1634, Naval Command, Control and Ocean Surveillance Center, RDT&E Division, San Diego, CA 92152-5001, Dec. 1993.

[18] Zeisse, C.R., "NAM6: Batch Code fo the Navy Aerosol Model," Technical Report 1804, SPAWAR Systems Center, San Diego, CA 92152-5001, Oct. 1999.

[19] Berk, A., G.P. Anderson, P.K. Acharya, J.H. Chetwynd, L.S. Bernstein, E.P. Shettle, M.W. Matthew, and S.M. Adler-Golden, "MODTRAN4 User's Manual," Air Force Research Laboratory, Hanscom AFB, MA (2000)

[20] Gerber, H.E., "Relative Humidity Parameterization of the Navy Aerosol Model (NAM)," NRL Report 8956, pg. 11, Naval Research Laboratory, Washington, DC (1985)

[21] Shettle, E.P., and R.W. Fenn, "Models for the Aerosols of the Lower Atmosphere and the Effects of Humidity Variations on Their Optical Properties," AFGL-TR-79-0214, Environmental Research Papers No. 676, AFGL, Hanscom AFB, MA (1979).

[22] Volz, F.E., J. Geophys. Res. **17**, 1017 (1972).

[23] Volz, F.E., Appl. Opt. **11**, 755 (1972).

[24] Hale, G.M. and M.R. Querry, Appl. Opt. **12**, 555 (1973)

[25] Sprangle, P., J.R. Peñano and B. Hafizi, Phys. Rev. E **66**, 046418 (2002)

[26] Peñano, J.R., P. Sprangle, B. Hafizi, A. Ting, D.F. Gordon, C.A. Kapetanakos, Phys. Plasmas **11**, 2865 (2004)

[27] "Handbook of Geophysics and the Space Environment," Air Force Geophysical Laboratory, Air Force Systems Command, A.D. Jursa, editor, 1985.